JOURNAL OF VIROLOGY, Jan. 2004, p. 779–789 Vol. 78, No. 2
0022-538X/04/$08.00+0 DOI: 10.1128/JVI.78.2.779–789.2004

Human Immunodeficiency Virus Type 1 Tat Regulates Endothelial Cell Actin Cytoskeletal Dynamics through PAK1 Activation and Oxidant Production

Ru Feng Wu,[1] Ying Gu,[1] You Cheng Xu,[1] Stefania Mitola,[2] Federico Bussolino,[2] and Lance S. Terada[1]*

The University of Texas Southwestern Medical Center and the Dallas Veterans Administration Medical Center, Dallas, Texas,[1] and The Institute for Cancer Research and Treatment and University of Turin, Turin, Italy[2]

Received 16 June 2003/Accepted 28 September 2003

Human immunodeficiency virus type 1 Tat exerts prominent angiogenic effects which may lead to a variety of vasculopathic conditions in AIDS patients. Because endothelial cells undergo prominent cytoskeletal rearrangement during angiogenesis, we investigated the specific effects of Tat on the endothelial cell actin cytoskeleton. Glutathione *S*-transferase (GST)–Tat, at a level of 200 ng/ml (equivalent to 52 ng of Tat/ml), caused stress fiber disassembly, peripheral retraction, and ruffle formation in human umbilical vein endothelial cells (HUVEC) and human lung microvascular endothelial cells. At 600 ng of GST-Tat/ml (157 ng of Tat/ml), actin structures were lost, and severe cytoskeletal collapse occurred. In contrast, GST-Tat harboring mutations within either the cysteine-rich or basic domains exerted minimal effects on the endothelial cytoskeleton. HUVEC expressing a DsRed-Tat fusion protein displayed similar actin rearrangements, followed by actin collapse, whereas neighboring nontransfected cells retained normal actin structures. Because active mutants of p21-activated kinase 1 (PAK1) induce identical changes in actin dynamics, we hypothesized that Tat exerts its cytoskeletal effects through PAK1. GST-Tat activated PAK1 within 5 min, and adenovirus delivery of a kinase-dead PAK1 [PAK1(K298A)] completely prevented cytoskeletal collapse induced by GST-Tat or DsRed-Tat and also blocked downstream activation of c-Jun N-terminal kinase. Further, GST-Tat increased phosphorylation of the NADPH oxidase subunit p47^{phox} and caused its rapid redistribution to membrane ruffles. PAK1(K298A) blocked p47^{phox} phosphorylation, and interference with NADPH oxidase function through superoxide scavenging or through expression of a transdominant inhibitor, p67(V204A), prevented GST-Tat-induced alterations in the actin cytoskeleton. We conclude that Tat induces actin cytoskeletal rearrangements through PAK1 and downstream activation of the endothelial NADPH oxidase.

The vascular endothelium of human immunodeficiency virus (HIV)-infected patients displays a number of morphological and functional abnormalities that are thought to contribute to the spectrum of AIDS-associated diseases. Chaotic endothelial cell morphology is seen in 94% of aortas of HIV type 1 (HIV-1)-infected patients (31), and abnormalities seen in pulmonary and coronary intima and in Kaposi's sarcoma cells suggest disorganized angiogenic behavior (18, 26). In this regard, the viral accessory protein Tat presents a likely candidate vasculopathic factor. Tat is found circulating in the blood of AIDS patients (28) and can enter uninfected cells through its protein transduction domain (24). In addition, Tat initiates outside-in signaling through receptor ligation, thus promoting endothelial cell migration and matrix invasion in vitro and angiogenesis in vivo (3, 4, 19, 23).

Although the angiogenic behavior stimulated by Tat has been well described, the signaling pathways underlying the accompanying endothelial cell morphological changes are poorly understood. Early during the response to other known angiogenic agents, such as vascular endothelial cell growth factor (VEGF), dramatic alterations in the endothelial cell actin cytoskeleton must occur to allow separation of interendothelial junctions and migration of cells to form vascular sprouts. Such actin cytoskeletal changes include ruffling of leading-edge membranes and depolymerization of trailing-edge stress fibers to allow treadmilling and locomotion to occur. Angiogenic endothelium also becomes leaky, since peripheral retraction occurs in conjunction with the breakdown of lateral intercellular junctions.

In the present study, we identify a signaling pathway through which HIV-1 Tat affects endothelial cell actin microfilament dynamics. Tat caused dramatic actin cytoskeletal rearrangements such as membrane ruffling, peripheral retraction, and subsequent cytoskeletal disassembly, which we found to be driven by activation of the MAP kinase kinase kinase kinase p21-activated kinase 1 (PAK1). In addition, involvement of an endothelial cell NADPH oxidase downstream of PAK1 appeared necessary for these cytoskeletal changes.

MATERIALS AND METHODS

Plasmid and adenovirus construction. All PCR amplifications were performed with either *Pfu* Turbo (Stratagene) or *Pfx* Platinum (Invitrogen), and all constructs were confirmed by sequencing. DsRed-Tat was derived by *Bam*HI exci-

* Corresponding author. Mailing address: Dallas VAMC, MC151, 4500 S. Lancaster Rd., Dallas, TX 75216. Phone: (214) 857-0405. Fax: (214) 857-0340. E-mail: lance.terada@med.va.gov.

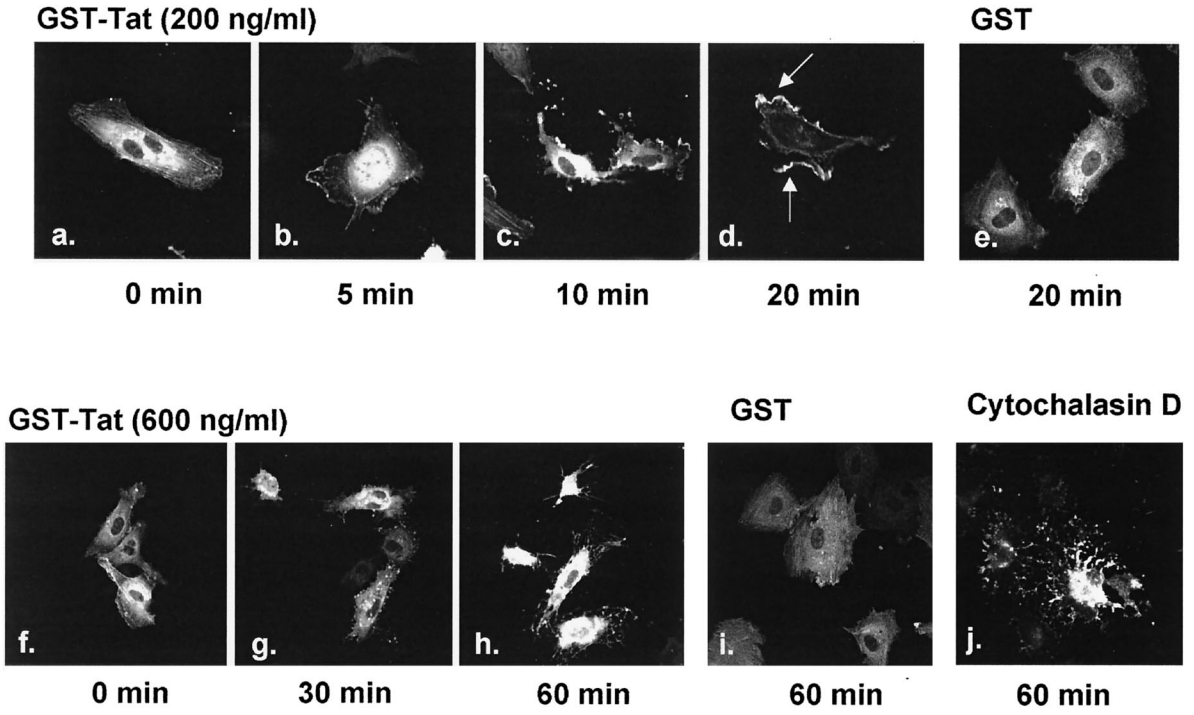

FIG. 1. Effect of GST-Tat on endothelial cell actin dynamics. (a) HUVEC were transfected with actin-GFP to visualize actin microfilament structures. Cells were subsequently treated with GST-Tat or GST alone for the indicated times and observed live and unfixed. At a concentration of 200 ng/ml, loss of stress fibers and peripheral retraction were seen within 5 min (b and c), and ruffling was observed within 5 min and peaking at approximately 20 min (b to d, arrows). (e) GST alone had no effect on actin structures. (g) At a concentration of 600 ng/ml, ruffling occurred early and was followed by the appearance of actin retraction fibers. (h) By 60 min, all cells showed marked collapse of the actin skeleton, with most cells displaying a reticular or a stellate cytosolic remnant. (i) Treatment with GST alone (600 ng/ml) had no effect on actin dynamics. Collapse of the actin cytoskeleton induced by cytochalasin D (10 μM) is shown in panel j for comparison.

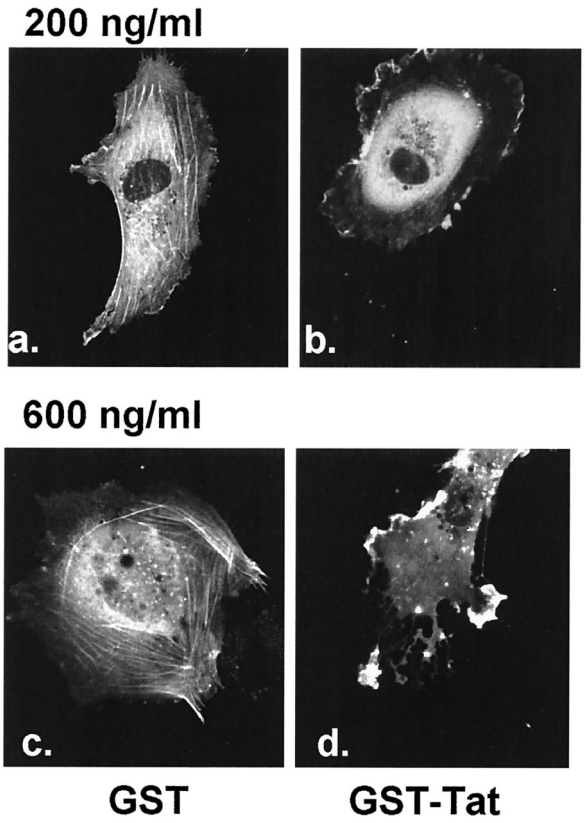

sion of HIV-1 Tat-86 from pGEX-Tat-86 (National Institutes of Health AIDS Research and Reference Reagent Program) and ligation into pDsRed2-C1 (Clontech). The full-length $p47^{phox}$ coding region was excised from pBluescript-SK and ligated into the *Eco*RI site of pDsRed2-C1 to create DsRed-p47. Human HA-JNK2 and pCINF-p47 (encoding Flag-p47) were constructed as previously described (29). Mutations in the cysteine-rich [GST-Tat C(22,25,27)A] or basic [GST-Tat R(49,52,53,55,56,57)A] domains of HIV-1 Tat were introduced as described previously (19). pEGFP and actin-green fluorescent protein (GFP) were purchased from Clontech. pCMV5 M-PAK1(K298A) was obtained from Melanie Cobb (University of Texas Southwestern), PCR amplified with addition of terminal *Nhe*I and *Sal*I sites, and ligated directionally into the corresponding sites of the shuttle vector pDC315io (Microbix) containing a loxP site and the murine cytomegalovirus promoter upstream of a *lac* operator site, to generate pDC315-PAK1(K298A). This plasmid was cotransfected with the adenovirus backbone pBHGlox(del)E1,3Cre (Microbix) containing a Cre recombinase cassette. To avoid potential interference with growth and survival signals in packaging cells due to overexpression of PAK1(K298A), transgene expression was suppressed by constitutive *lac* repressor expression by the packaging cell line 293IQ (Microbix). Viral plaques were cloned and titers were determined by using 293IQ cells. The p67(V204A) mutation, previously constructed from $p67^{phox}$ (11), was excised and ligated into the *Eco*RI site of the shuttle vector pDC316io (Microbix). Viruses were again produced after Cre-Lox

FIG. 2. Effect of GST-Tat on HLMVEC. (a and c) Unstimulated HLMVEC or GST-treated HLMVEC transfected with actin-GFP displayed pronounced flattening and prominent stress fibers. (b) After treatment with 200 ng of GST-Tat/ml, stress fibers resorbed and edge ruffles appeared within 20 to 30 min, similar in character to changes observed in HUVEC. (d) At 600 ng of GST-Tat/ml, actin collapse and focal edge accumulation were seen.

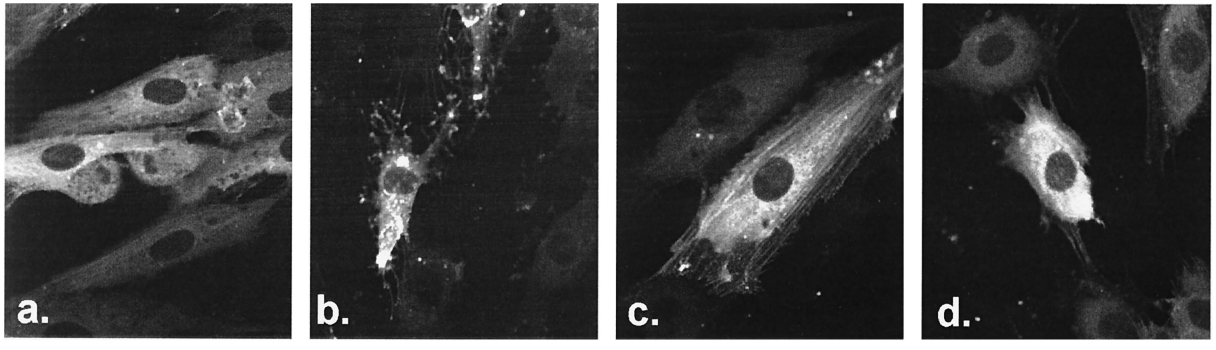

FIG. 3. Effect of Tat basic and cysteine-rich domains. HUVEC were transfected with actin-GFP and exposed to 600 ng of GST/ml (a), wild-type GST-Tat (b), GST-Tat R(49,52,53,55,56,57)A (c), or GST-Tat C(22,25,27)A (d). Whereas all cells exposed to wild-type GST-Tat displayed marked cytoskeletal collapse, cells exposed to GST-Tat containing mutations within the basic domain remained identical to GST-treated cells. Rare cells treated with the cysteine-rich domain mutant GST-Tat developed retraction fibers.

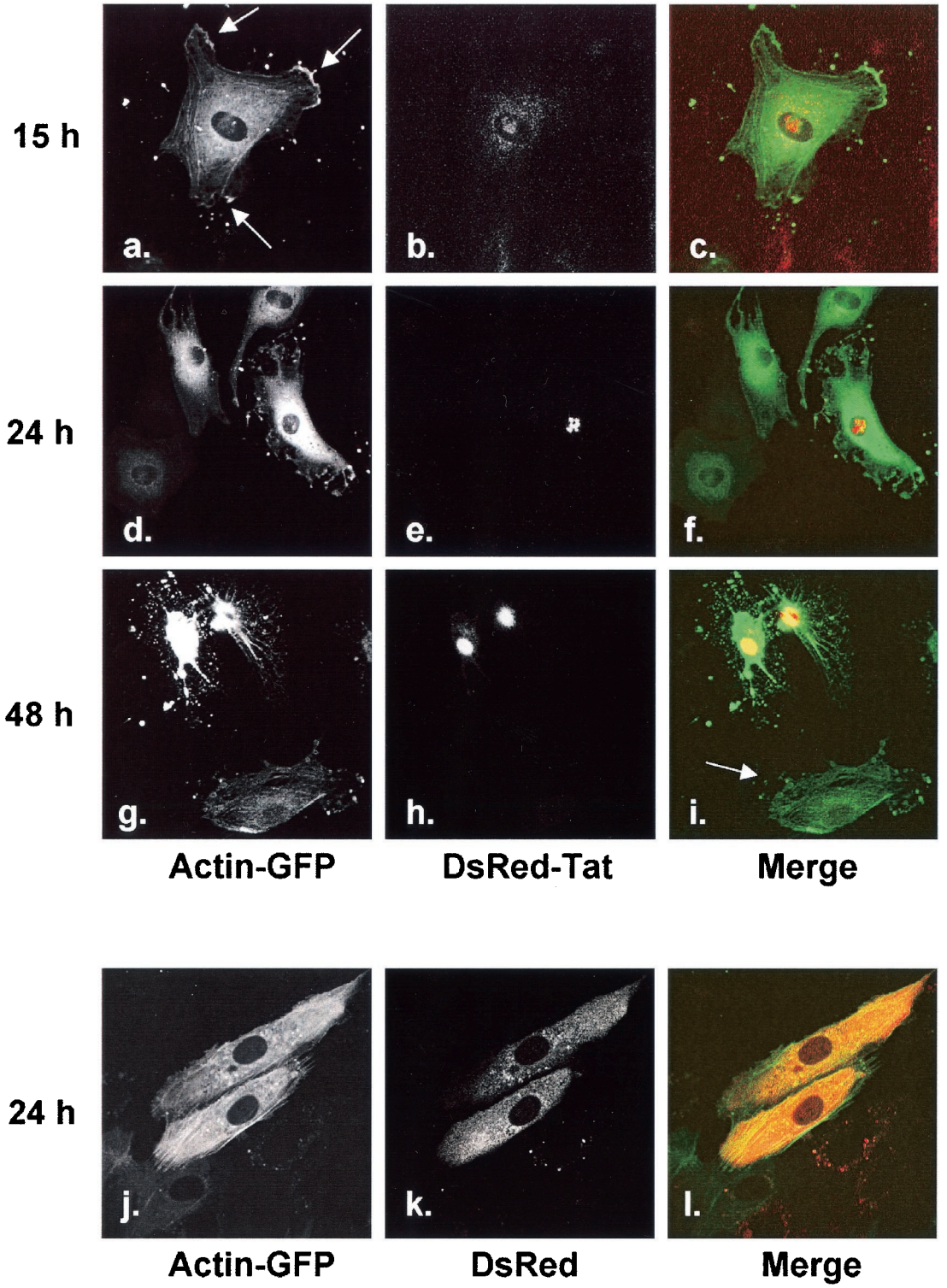

FIG. 4. Effect of DsRed-Tat on endothelial cell actin dynamics. HUVEC were cotransfected with actin-GFP and DsRed-Tat and observed at the indicated times. Actin-GFP was imaged in the green channel (a, d, g, and j), and DsRed-Tat or DsRed was imaged in the red channel (b, e, h, and k). At 15 h, frequent ruffle formation was observed (a, arrows), and DsRed-Tat was seen accumulating in nucleoli, with occasional visualization in cytosol (b). Peripheral retraction started within 24 h (d), seen in DsRed-Tat-expressing cells (d to f). (g to i) By 48 h, DsRed-Tat-expressing cells displayed actin collapse identical to that after GST-Tat treatment. Actin changes were visualized only in DsRed-Tat-expressing cells and not in neighboring cells (i, arrow). Cells transfected with DsRed alone did not exhibit alterations in actin dynamics at 24 h (j to l) or 48 h (not shown).

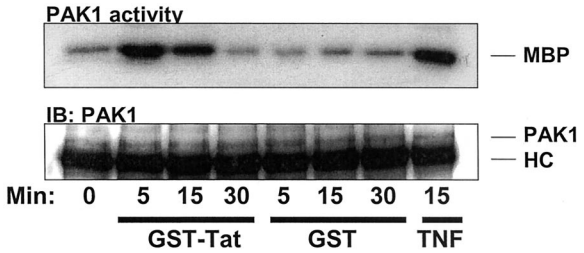

FIG. 5. Activation of PAK1 by GST-Tat. HUVEC were treated with GST-Tat or GST (600 ng/ml) for the indicated times. PAK1 activation was assessed by IP kinase and phosphorylation of myelin basic protein (MBP). TNF (100 ng/ml) was added for 15 min as a positive control. The lower panel shows an immunoblot of immunoprecipitated PAK1 with anti-PAK1. HC, immunoglobulin heavy chain.

recombination in 293IQ cells. The Ad-lacZ virus was as previously described (29).

GST-Tat production. SURE *Escherichia coli* (Stratagene) was transformed with pGEX-2TK, pGEX-Tat-86, pGEX-Tat C(22,25,27)A, or pGEX-Tat R(49,52,53,55,56,57)A and was induced with IPTG (isopropyl-β-D-thiogalactopyranoside) for 3 to 4 h at 37°C, and the fusion proteins were extracted as previously described (10, 29), keeping all solutions degassed and at 4°C. The yield, stability, and biological activity of wild-type Tat (assessed as activation of endothelial cell c-Jun N-terminal kinase [JNK]) were highest when flash-frozen as a glutathione *S*-transferase (GST) fusion.

Cell culture and transduction. Human umbilical vein endothelial cells (HUVEC) were obtained from BioWhittaker, grown in EGM-2 media, and used within five passages. Human lung microvascular endothelial cells (HLMVEC) were obtained from BioWhittaker, grown in EGM-2-MV media, and used on the first passage. Transfection was performed by electroporation after thymidine-induced cell cycle synchronization as previously described (29). Adenovirus transduction was achieved after infection of HUVEC at 70 to 90% confluence for 1 h at a multiplicity of infection (MOI) of 100:1, followed by a 24-h recovery period in full media. In some experiments, cells were pretreated with the superoxide dismutase mimetic Mn(III) tetrakis(1-*methyl*-4-pyridil)porphyrin (MnTMPyP; Alexis) at 100 μM for 1 h.

Microscopy. HUVEC were plated on fibronectin-coated coverslip chambers (Nunc), and live cells were observed on a heated stage without fixation or permeabilization. Confocal images were obtained with an inverted Zeiss Axiovert S100TV microscope and the LSM 410 laser-scanning system. Fluorescence ratio imaging was performed by using Zeiss LSM (v3.98) software.

Kinase activities. PAK1 activity was assessed by an immunoprecipitation kinase method. After treatment, HUVEC were harvested in cold lysis buffer (20 mM Tris-HCl [pH 7.5], 150 mM NaCl, 1 mM disodium EDTA, 1 mM EGTA, 1% Triton X-100, 2.5 mM sodium pyrophosphate, 1 mM β-glycerophosphate, 1 mM Na_3VO_4, 1 μg of leupeptin/ml, and 1 mM phenylmethylsulfonyl fluoride), sonicated briefly, and immunoprecipitated with rabbit anti-PAK1 (Santa Cruz). The kinase reaction was performed with 5 μg of myelin basic protein (Upstate) as a PAK1 substrate in the presence of [γ^{32}P]ATP (Perkin-Elmer) at 30°C for 30 min. For JNK activity, HUVEC were cotransfected with HA-JNK2 and either PAK1(K298A) or empty vector. The following day, an immunocomplex assay was performed with anti-HA (Santa Cruz) and 2 μg of GST-Jun as a substrate (29). Two-thirds of each sample was subjected to autoradiography, and one-third was subjected to immunoblot to assess capture of PAK1 or HA-JNK2.

p47^{phox} phosphorylation. HUVEC were cotransfected with Flag-p47 and either PAK1(K298A) or empty vector, and the following day the medium was replaced with phosphate-free Dulbecco modified Eagle medium (Sigma) containing 0.5 mCi of [^{32}P]orthophosphate/ml for 4 h. Cells were then stimulated with GST or GST-Tat (600 ng/ml) for 15 min and lysed on ice for 15 min in lysis buffer containing 0.1% sodium dodecyl sulfate and 0.5% deoxycholate. After it was sheared through a 23-gauge needle 10 times, the 13,000 × *g* supernatant was precleared and normalized for protein. Flag-p47 was immunoprecipitated with anti-Flag and washed four times in lysis buffer with sodium dodecyl sulfate and deoxycholate, twice in lysis buffer containing 0.5 M NaCl, and once in 50 mM Tris (pH 7.0). One-third of the immunoprecipitate was immunoblotted for p47^{phox} to assess capture and loading, and the remainder was analyzed by autoradiography.

RESULTS

GST-Tat induces prominent actin cytoskeletal rearrangement. Actin structures were visualized in live cells by using actin-GFP. After treatment of HUVEC with 200 ng of GST-Tat/ml (corresponding to 52 ng of Tat)/ml, stress fibers were seen to diminish within 5 to 10 min (Fig. 1b). Within 10 min and peaking at 15 to 25 min, various amounts of peripheral retraction (Fig. 1c) and prominent ruffling (Fig. 1d) were observed. Membrane ruffles are vertical actin scaffolds that accompany cell movement and were recognized by their characteristic morphology, rapid movement across cells, and dorsal projection. Tat-induced ruffles were frequently disorganized, causing multiple leading edges to form and dissipate (e.g., Fig. 1d). Ruffling diminished within 1 h. Cells treated with GST alone did not change within this time frame (Fig. 1e).

Treatment of HUVEC with 600 ng of GST-Tat/ml (corresponding to 157 ng of Tat/ml) induced early ruffling but within 30 min led to prominent actin retraction fibers as the cell periphery contracted (Fig. 1g). After 60 min, the HUVEC actin skeleton collapsed in virtually all cells, leaving a trabeculated, arborized cytosolic remnant (Fig. 1h). Collapse of the actin skeleton was confirmed by comparison with cytochalasin D-treated cells, which mimicked the Tat-induced arborized pattern (Fig. 1j). Despite the severe cytoskeletal disruption, however, the nuclear morphology was unchanged. Again, treatment with 600 ng of GST/ml alone had no effect on actin structures (Fig. 1i). The cytoskeletal effects of GST-Tat were also observed in HLMVEC, suggesting that activation of these pathways was not confined to HUVEC. Within 20 to 30 min of GST-Tat treatment (200 ng/ml), prominent stress fibers within HLMVEC were disassembled (Fig. 2a and b). At the higher dose (600 ng/ml), GST-Tat caused both collapse of the normal actin skeleton and scattered lamellar formations (Fig. 2d).

HIV-1 Tat possesses several known functional domains, including a cysteine-rich putative dimerization motif and a polybasic domain involved in growth factor receptor recognition. These latter two domains are both critical to Tat-induced autophosphorylation of VEGFR-2 and chemotactic migration of endothelial cells in response to Tat (19), a response that requires active cytoskeletal reorganization. Thus, we tested the involvement of these two functional domains in altering actin dynamics. We found that, whereas wild-type GST-Tat induced marked actin changes within 60 min, GST-Tat R(49,52, 53,55,56,57)A had no discernible effects on actin structure, even at 600 ng/ml, in any cell observed (Fig. 3a to c). At 600 ng/ml, GST-Tat C(22,25,27)A caused very little cytoskeletal movement, with rare cells displaying actin retraction fibers but no membrane ruffling (Fig. 3d). Thus, both the basic and cysteine-rich domains appear necessary for Tat to initiate the observed actin rearrangements.

To further confirm the influence of Tat on actin dynamics, HUVEC were transfected with DsRed-Tat, allowing comparison of Tat-expressing versus nonexpressing cells. We found early and prominent nucleolar localization of DsRed-Tat but visualized cytosolic DsRed-Tat in occasional cells as well (Fig. 4a to c). At 15 h, membrane ruffling was observed in DsRed-Tat-expressing cells. By 24 h, DsRed-Tat expression was generally higher, and cells exhibited loss of stress fibers and marked peripheral retraction (Fig. 4d to f). By 48 h, DsRed-

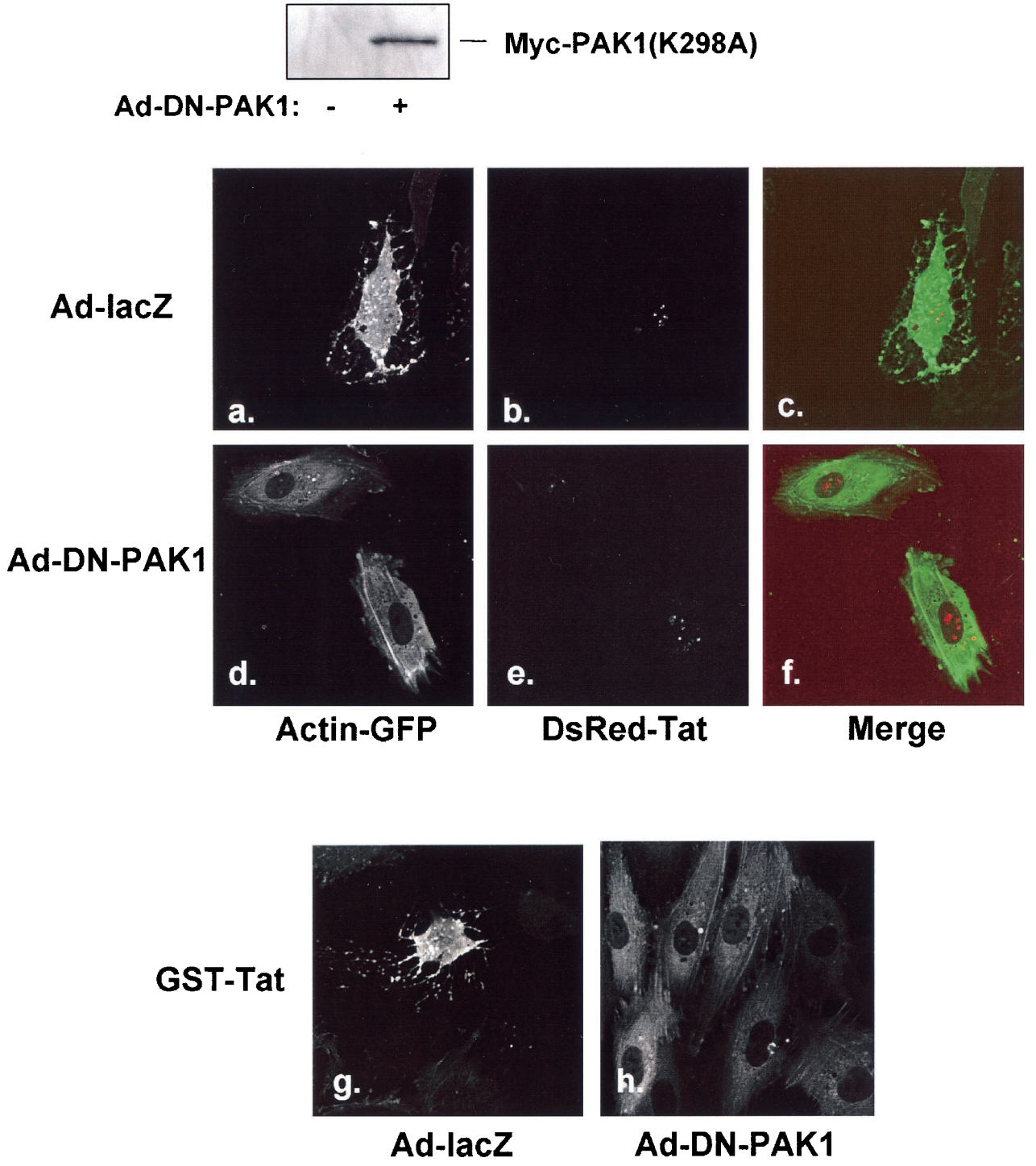

FIG. 6. Effect of PAK1(K298A) on actin rearrangement. HUVEC were cotransfected with actin-GFP and DsRed-Tat and then infected with either Ad-lacZ or Ad-PAK1(K298A) (MOI = 100:1, 1 h) the following day. Cells were examined after 48 h. The upper panel shows immunoblot with anti-Myc, demonstrating expression of Myc-tagged PAK1(K298A) (DN-PAK1). Actin-GFP was imaged in the green channel (a and d), and DsRed-Tat was imaged in the red channel (b and e). DsRed-Tat-expressing cells infected with Ad-lacZ displayed prominent actin collapse (a to c), whereas DsRed-Tat-expressing cells infected with Ad-PAK1(K298A) retained normal morphology (d to f). (g and h) HUVEC were transfected with actin-GFP, infected with the corresponding adenoviruses, and treated with GST-Tat (600 ng/ml for 60 min). GFP-actin is shown. Cytoskeletal collapse seen in Ad-lacZ-infected cells was absent in Ad-PAK1(K298A)-infected cells.

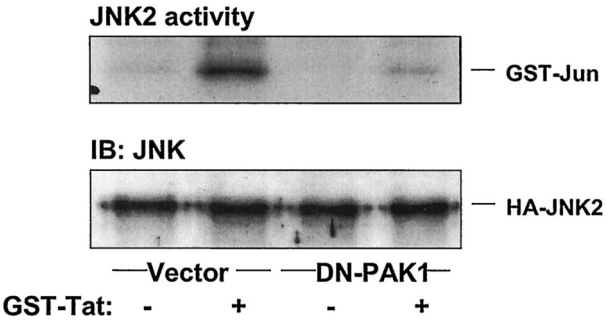

FIG. 7. Effect of PAK1(K298A) on JNK activation. HUVEC were cotransfected with either empty vector or PAK1(K298A) (DN-PAK1), and with HA-JNK2. After 24 h, cells were treated with GST-Tat (600 ng/ml, 15 min), and HA-JNK2 activation was assessed by IP kinase. Capture of HA-JNK2 was assessed by immunoblotting for JNK (lower panel). PAK1(K298A) blocked JNK activation by GST-Tat.

Tat-expressing cells acquired a collapsed actin skeleton with dendritic cytosolic projections, identical to cells treated with 600 ng of GST-Tat (Fig. 4g to i)/ml. Notably, cytoskeletal abnormalities were restricted to DsRed-Tat-expressing cells, whereas neighboring cells displayed normal actin structures and no visible DsRed-Tat (Fig. 4g to i). Thus, we did not find evidence that DsRed-Tat could be exported and internalized by other cells diffusely. DsRed not fused to Tat was confined to the cytosol and did not affect actin dynamics (Fig. 4j to l). Hence, the ability of Tat to cause dramatic rearrangements in the actin cytoskeleton did not appear to be an artifact of of DsRed itself, or of the GST fusion tag or preparative contaminants.

PAK1 transduces GST-Tat-induced cytoskeletal rearrangements. The morphology of the collapsed actin structures precipitated by exogenous or expressed Tat is highly reminiscent of actin dynamics seen after microinjection of active PAK1 mutants into HeLa and Ref52 cells (8, 16, 30). Accordingly, we hypothesized that Tat may exert its cytoskeletal effects through activation of endothelial PAK1. We found robust activation of PAK1 in HUVEC within 5 min of exposure to GST-Tat, decreasing by 30 min, whereas GST alone had no effect (Fig. 5). PAK1 activation by GST-Tat was at least as strong as with the known PAK1 agonist TNF (Fig. 5, right lane).

To test the involvement of PAK1 in Tat-induced cytoskeletal dynamics, we generated an adenovirus harboring the kinase-dead mutant PAK1(K298A), which possesses dominant-interfering activity (8). Efficiency of adenovirus-dependent transduction in HUVEC, assessed by in situ β-galactosidase staining after Ad-lacZ infection, was in excess of 95% (not shown). Transgene expression was demonstrated by immunoblot for the Myc-tagged PAK1(K298A) (Fig. 6, top panel). We found that expression of PAK1(K298A) essentially abolished Tat-induced cytoskeletal rearrangements. Whereas all DsRed-Tat-expressing cells displayed various degrees of actin cytoskeletal disruption when infected with the control virus Ad-lacZ (Fig. 6a to c), Ad-PAK1(K298A)-infected cells had quiescent actin skeletons, many with well-formed stress fibers, even while expressing DsRed-Tat (Fig. 6d to f). More remarkably, addition of 600 ng of GST-Tat/ml, which induced cell collapse in virtually all cells infected with Ad-lacZ, did not increase ruffle formation or induce actin collapse in PAK1(K298A)-transduced cells observed well beyond 60 min (Fig. 6g and h). As further evidence that Tat initiates angiogenic signal pathways through PAK1, we examined activation of the JNK mitogen-activated protein kinase (MAPK), which is known to mediate proliferative and angiogenic signaling downstream of VEGF receptor ligation (22). As with the cytoskeletal changes, PAK1(K298A) effectively abolished JNK2 activation by GST-Tat (Fig. 7).

An NADPH oxidase acts upstream of GST-Tat-induced cytoskeletal rearrangements. We previously demonstrated that HIV-1 Tat increases oxidant production in endothelial cells through activation of a phagocyte-like NADPH oxidase and that Tat-induced activation of the JNK MAPK occurs through such oxidants (10). Further, the NADPH oxidase adapter $p47^{phox}$ was found to be constitutively associated with the endothelial cell cytoskeleton (12). We therefore sought to determine whether the endothelial oxidase participates in Tat-induced actin cytoskeletal changes. We found first that treatment of HUVEC with GST-Tat caused redistribution of $p47^{phox}$ to membrane ruffles within 15 to 20 min. DsRed-p47 localized to actin-GFP-containing ruffles upon stimulation with GST-Tat but not GST alone (Fig. 8a to f). Fluorescence ratio imaging revealed cancellation of red and green intensities within ruffles, further demonstrating colocalization of the two chromophores (Fig. 8g). In contrast, DsRed itself did not concentrate within Tat-induced ruffles (Fig. 8h to j); green/red ratio images therefore displayed prominent enhancement of actin-GFP within ruffles relative to DsRed (Fig. 8k).

In phagocytes, phosphorylation of $p47^{phox}$ initiates assembly and activation of the NADPH oxidase (2). We found that GST-Tat increased phosphorylation of Flag-p47 within 15 min by ~5-fold (average of two independent experiments), whereas GST alone did not (Fig. 9), a finding consistent with our prior observations that Tat activates an endothelial cell NADPH oxidase (10). Unlike the situation in phagocytes, detectable basal phosphorylation of $p47^{phox}$ was observed. Expression of PAK1(K298A) effectively blocked both basal and Tat-stimulated $p47^{phox}$ phosphorylation, demonstrating that PAK1 acts upstream of $p47^{phox}$.

To test for involvement of the NADPH oxidase in actin rearrangements, we constructed a second adenovirus delivering the oxidase-activating subunit $p67^{phox}$ harboring a mutation in the purported activation domain. This mutant, p67(V204A), decreases oxidant production in the presence of wild-type $p67^{phox}$, thus possessing dominant-negative activity (13). Expression of p67(V204A), confirmed by immunoblotting (Fig. 10 top panel), completely blocked actin cytoskeletal collapse in GST-Tat-treated HUVEC (Fig. 10a to d). Further, treatment of cells with the membrane permeant superoxide dismutase mimetic MnTMPyP also completely blocked cytoskeletal collapse (Fig. 10e to f), confirming a role for oxidants in the control of actin dynamics by Tat.

DISCUSSION

Known angiogenic factors such as VEGF, basic FGF, and angiopoietin-1 induce characteristic changes in actin dynamics

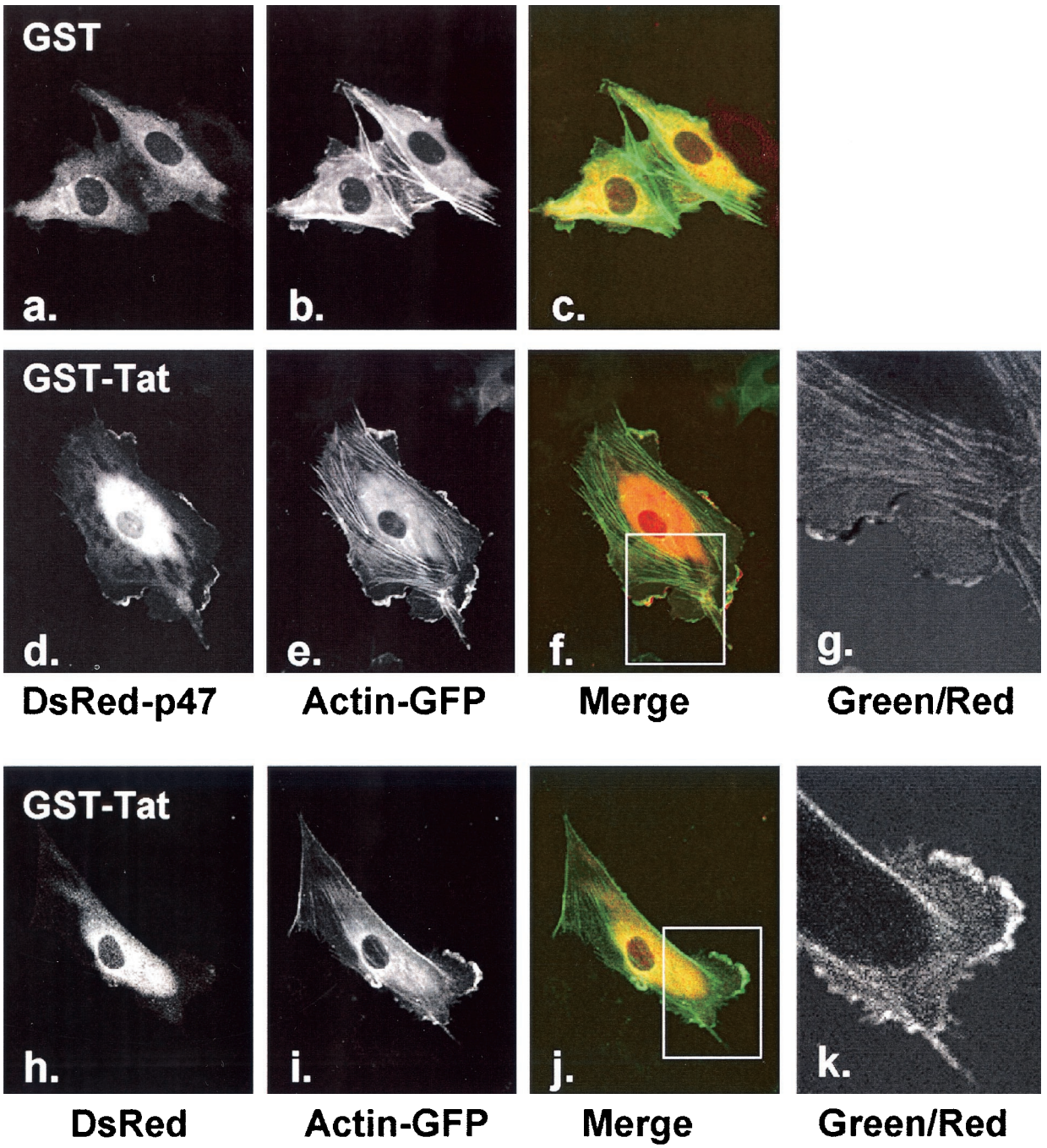

FIG. 8. DsRed-p47 translocates to Tat-induced membrane ruffles. HUVEC were cotransfected with actin-GFP and DsRed-p47. After stimulation of cells with GST (a to c) or GST-Tat (d to g) (200 ng/ml, 15 to 20 min), DsRed-p47 was imaged in the red channel (a and d), and actin-GFP was imaged in the green channel (b and e). DsRed-p47 translocated avidly to actin ruffles upon stimulation with GST-Tat (d to f). The green/red fluorescence ratio image of inset from panel f shows cancellation of actin-GFP signal by DsRed-p47 within ruffles (g), indicating colocalization of the two proteins. DsRed itself, when cotransfected with actin-GFP, did not translocate to ruffles (h to j). The green/red ratio image of inset from panel j shows relative enhancement of actin-GFP within ruffle relative to DsRed (k).

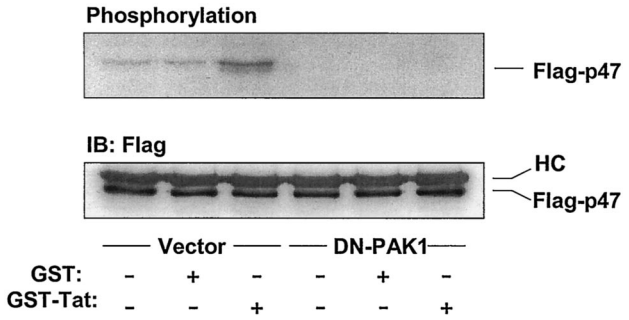

FIG. 9. Effect of PAK1(K298A) on p47^{phox} phosphorylation. HUVEC were cotransfected with either empty vector or PAK1(K298A) (DN-PAK1) and with Flag-p47 and then stimulated with GST or GST-Tat (600 ng/ml). Flag-p47 was immunoprecipitated, and phosphorylation (upper panel) and protein capture (anti-Flag, lower panel) were assessed. GST-Tat increased phosphorylation of p47^{phox}, whereas PAK1(K298A) completely blocked basal and Tat-induced p47^{phox} phosphorylation.

leading to membrane ruffling and dissolution of stress fibers with redistribution of focal adhesions. These cytoskeletal changes are currently thought to facilitate migration and invasion of endothelial cells during sprout formation. In the present study, we found that HIV-1 Tat induced rapid and dramatic changes in the actin cytoskeleton consistent with its known biological effect as a proangiogenic agent.

Extracellular Tat delivered as a GST fusion increased ruffle formation and peripheral retraction and at higher levels caused prominent loss of stress fibers with visible depolymerization and collapse of the actin cytoskeleton. These dramatic effects on actin dynamics are consistent with physiologic and biochemical studies demonstrating an increase in paracellular albumin permeability (21) and in phosphorylation of focal adhesion proteins such as FAK, Pyk2, paxillin, and p130^{Cas} (9) after Tat treatment. Interestingly, cellular expression of Tat as a DsRed fusion produced identical morphological changes, raising questions about the site of the molecular target(s) of Tat involved in cytoskeletal alterations. The appearance of normal cells in close proximity to collapsed, DsRed-Tat-expressing cells suggests that Tat may bind intracellular target proteins to effect such changes rather than being exported and acting in a paracrine fashion. This suggests other mechanisms for cytoskeletal signaling beyond ligation of known Tat receptors such as VEGFR2 and $\alpha_V\beta_3/\alpha_5\beta_1$ integrins (5, 23), although in the present study we have not excluded a receptor-mediated mechanism. An additional curiosity is that an intracellular site of action would be expected to reside within the cytosol or internal membrane surface, whereas DsRed-Tat accumulated in endothelial cell nucleoli. However, a cytosolic phase for DsRed-Tat was clearly seen in a fraction of cells, suggesting an equilibrium between nucleus and cytosol. This possibility is consistent with trafficking of a GFP-Tat protein, which also accumulates in nucleoli of HeLa cells (25). In this latter study, analysis of membrane fusion between transfected and nontransfected cells by using polyethylene glycol clearly demonstrated continuous shuttling of GFP-Tat between the nucleus and cytoplasm of HeLa cells.

Although the proximal molecular target of Tat responsible for initiating cytoskeletal changes is unknown, our data suggest early involvement of PAK1. PAK1, an MAP kinase kinase kinase kinase involved in mitogenic stimulation, is known to concentrate in membrane ruffles, and active mutants of PAK1 cause ruffle formation (7, 8). When expressed in extremely high levels achieved by microinjection, active PAK1 mutants—containing deletions or mutations in the autoinhibitory domain or fusion with active Cdc42—stimulate peripheral retraction, followed by actin depolymerization and collapse of the cytoskeleton (8, 16, 30), highly reminiscent of our findings with Tat. To our knowledge, such severe architectural derangements have not been previously observed without microinjection of these PAK1 mutants or cytochalasin treatment.

The relevance of PAK1 activation by Tat to HIV-1-infected patients may extend to tumor biology as well as AIDS vasculopathy. In tumor cells, PAK1 promotes migration and invasive behavior (1). Notably, Tat-expressing adenocarcinoma cells injected into mice produce aggressive, highly metastatic tumors (6), suggesting an active PAK1 phenotype and consistent with the biologically aggressive malignancies AIDS patients develop. In addition, during angiogenesis, endothelial cell behavior recapitulates that of tumor cells, becoming invasive, metastatic, and proliferative. Thus, angiogenic behavior may logically be linked to PAK1. Indeed, PAK1 has been linked to endothelial cell migration and contractility in vitro and angiogenesis in vivo (15, 17). The ability of Tat to activate endothelial PAK1 is therefore consistent with the intense angiogenesis invoked by Tat-secreting tumors and also with the development of invasive Kaposi's sarcoma-like vascular lesions in Tat-transgenic mice (6, 27). Accordingly, in AIDS-related Kaposi's sarcoma, the malignant vascular cells migrate and invade much more aggressively than in non-HIV-related Kaposi's sarcoma.

Recently, we demonstrated that Tat activates an NADPH oxidase upstream of the JNK MAPK in endothelial cells (10). In addition, p47^{phox}, the adapter subunit of this oxidase, was found to be constitutively associated with the cytoskeleton, and disruption of the actin cytoskeleton blocked Tat-induced signaling (10, 12), suggesting a functional relationship between the oxidase and the cytoskeleton. In the present study, our data suggest that activation of the endothelial NADPH oxidase occurs upstream of Tat-induced actin rearrangements. Exogenous oxidants are known to cause actin reorganization, and endogenous oxidants appear to be necessary for spontaneous endothelial cell migration (20). Thus, PAK1 may in part exert its cytoskeletal effects through NADPH oxidase activation, a premise supported by the dependence of p47^{phox} phosphorylation on PAK1 kinase activity. Notably, Tat induced translocation of p47^{phox} to membrane ruffles. These actin structures are known to be enriched in active PAK1, and oxidant production is focally produced in the ruffles of motile endothelial cells as well as phagocytes (14, 20). Finally, the demonstration that PAK1(K298A) blocked Tat-induced JNK activation is consistent with our prior observation that the NADPH oxidase also lies upstream of JNK activation by Tat (10). Thus, activation of PAK1 and the oxidase appear to control HIV-1 Tat signaling to both MAPK and cytoskeletal pathways.

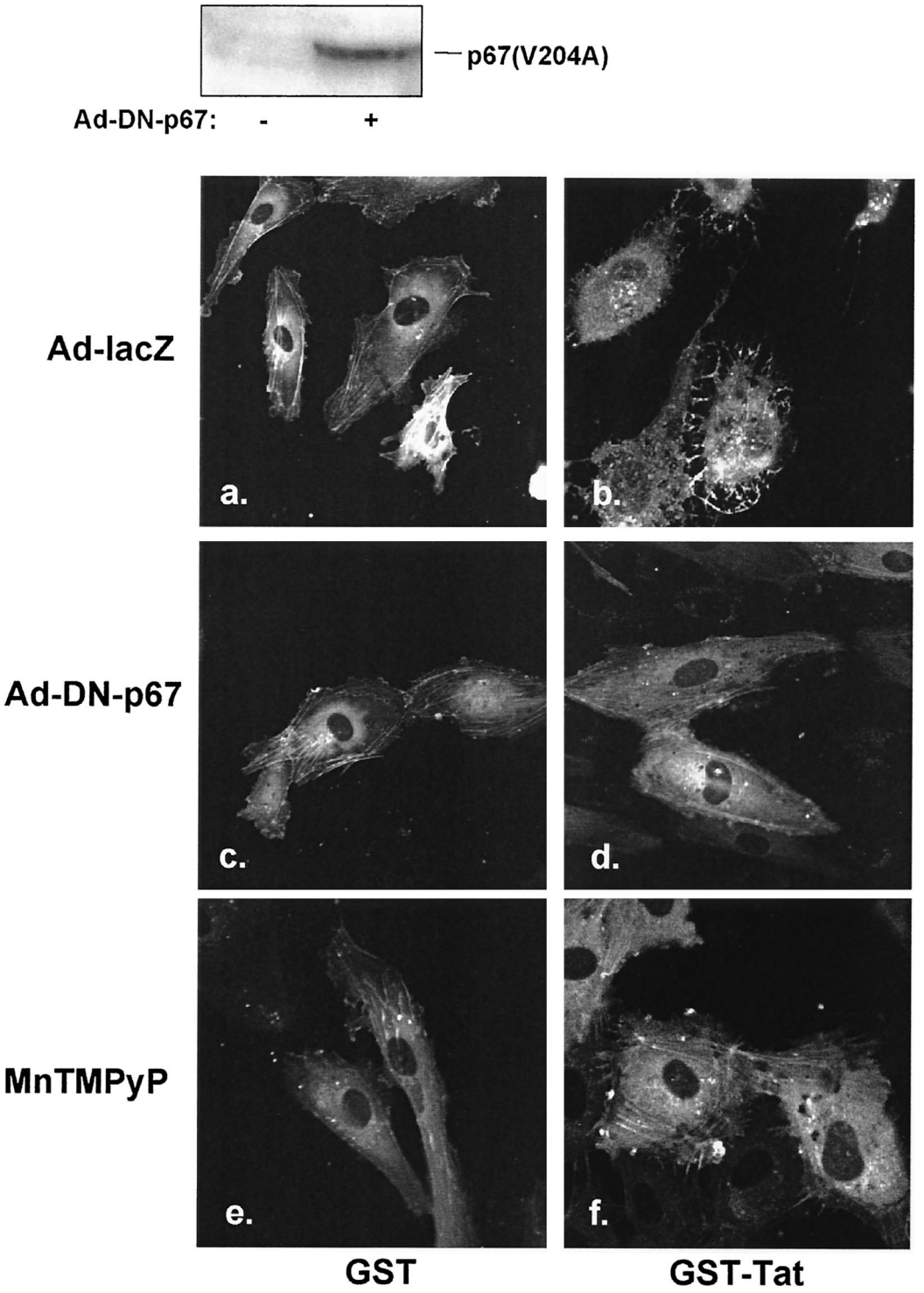

FIG. 10. Effect of p67(V204A) on actin rearrangement. HUVEC were transfected with actin-GFP and then infected with Ad-lacZ (a and b) or Ad-p67(V204A) (c and d) (MOI = 100:1, 1 h). The upper panel shows immunoblot with anti-$p67^{phox}$, demonstrating expression of p67(V204A) (DN-p67). (b) Cells infected with Ad-lacZ displayed prominent retraction and actin collapse after treatment with GST-Tat (600 ng/ml). (c and d) Expression of p67(V204A) completely suppressed actin cytoskeletal rearrangements. (e and f) HUVEC were transfected with actin-GFP and then pretreated with the superoxide dismutase mimetic MnTMPyP (100 μM, 1 h) prior to treatment with GST-Tat (600 ng/ml). MnTMPyP prevented the actin cytoskeletal changes induced by GST-Tat (f).

ACKNOWLEDGMENTS

We acknowledge the excellent technical assistance of Ginny Poffenberger.

This study was supported by NIH grants R01-HL061897 and R01-HL067256 and by the Veterans Administration.

REFERENCES

1. **Adam, L., R. Vadlamudi, M. Mandal, J. Chernoff, and R. Kumar.** 2000. Regulation of microfilament reorganization and invasiveness of breast cancer cells by kinase dead p21-activated kinase-1. J. Biol. Chem. **275:**12041–12050.
2. **Ago, T., H. Nunoi, T. Ito, and H. Sumimoto.** 1999. Mechanism for phosphorylation-induced activation of the phagocyte NADPH oxidase protein $p47^{phox}$: triple replacement of serines 303, 304, and 328 with aspartates disrupts the SH3 domain-mediated intramolecular interaction in $p47^{phox}$, thereby activating the oxidase. J. Biol. Chem. **274:**33644–33653.
3. **Albini, A., G. Barillari, R. Benelli, R. C. Gallo, and B. Ensoli.** 1995. Angiogenic properties of human immunodeficiency virus type 1 Tat protein. Proc. Natl. Acad. Sci. USA **92:**4838–4842.
4. **Albini, A., R. Soldi, D. Giunciuglio, E. Giraudo, R. Benelli, L. Primo, D. Noonan, M. Salio, G. Camussi, W. Rockl, and F. Bussolino.** 1996. The angiogenesis induced by HIV-1 tat protein is mediated by the Flk-1/KDR receptor on vascular endothelial cells. Nat. Med. **2:**1371–1375.
5. **Barillari, G., C. Sgadari, V. Fiorelli, F. Samaniego, S. Colombini, V. Manzari, A. Modesti, B. C. Nair, A. Cafaro, M. Sturzl, and B. Ensoli.** 1999. The Tat protein of human immunodeficiency virus type-1 promotes vascular cell growth and locomotion by engaging the $\alpha_5\beta_1$ and $\alpha_v\beta_3$ integrins and by mobilizing sequestered basic fibroblast growth factor. Blood **94:**663–672.
6. **Corallini, A., D. Campioni, C. Rossi, A. Albini, L. Possati, M. Rusnati, G. Gazzanelli, R. Benelli, L. Masiello, V. Sparacciari, M. Presta, F. Mannello, G. Fontanini, and G. Barbanti-Brodano.** 1996. Promotion of tumour metastases and induction of angiogenesis by native HIV-1 Tat protein from BK virus/tat transgenic mice. AIDS **10:**701–710.
7. **Dharmawardhane, S., A. Schurmann, M. A. Sells, J. Chernoff, S. L. Schmid, and G. M. Bokoch.** 2000. Regulation of macropinocytosis by p21-activated kinase-1. Mol. Biol. Cell **11:**3341–3352.
8. **Frost, J. A., A. Khokhlatchev, S. Stippec, M. A. White, and M. H. Cobb.** 1998. Differential effects of PAK1-activating mutations reveal activity-dependent and -independent effects on cytoskeletal regulation. J. Biol. Chem. **273:**28191–28198.
9. **Ganju, R. K., N. Munshi, B. C. Nair, Z. Y. Liu, P. Gill, and J. E. Groopman.** 1998. Human immunodeficiency virus tat modulates the Flk-1/KDR receptor, mitogen-activated protein kinases, and components of focal adhesion in Kaposi's sarcoma cells. J. Virol. **72:**6131–6137.
10. **Gu, Y., R. F. Wu, Y. C. Xu, S. C. Flores, and L. S. Terada.** 2001. HIV Tat activates c-Jun amino-terminal kinase through an oxidant-dependent mechanism. Virology **286:**62–71.
11. **Gu, Y., Y. C. Xu, R. F. Wu, F. E. Nwariaku, R. F. Souza, S. C. Flores, and L. S. Terada.** 2003. $p47^{phox}$ participates in activation of RelA in endothelial cells. J. Biol. Chem. **278:**17210–17217.
12. **Gu, Y., Y. C. Xu, R. F. Wu, R. F. Souza, F. E. Nwariaku, and L. S. Terada.** 2002. TNF alpha activates c-Jun amino terminal kinase through $p47^{phox}$. Exp. Cell Res. **272:**62–74.
13. **Han, C. H., J. L. Freeman, T. Lee, S. A. Motalebi, and J. D. Lambeth.** 1998. Regulation of the neutrophil respiratory burst oxidase: identification of an activation domain in $p67^{phox}$. J. Biol. Chem. **273:**16663–16668.
14. **Heyworth, P. G., J. M. Robinson, J. Ding, B. A. Ellis, and J. A. Badwey.** 1997. Cofilin undergoes rapid dephosphorylation in stimulated neutrophils and translocates to ruffled membranes enriched in products of the NADPH oxidase complex. Evidence for a novel cycle of phosphorylation and dephosphorylation. Histochem. Cell Biol. **108:**221–233.
15. **Kiosses, W. B., J. Hood, S. Yang, M. E. Gerritsen, D. A. Cheresh, N. Alderson, and M. A. Schwartz.** 2002. A dominant-negative p65 PAK peptide inhibits angiogenesis. Circ. Res. **90:**697–702.
16. **Manser, E., H.-Y. Huang, T.-H. Loo, X.-Q. Chen, J.-M. Dong, T. Leung, and L. Lim.** 1997. Expression of constitutively active α-PAK reveals effects of the kinase on actin and focal complexes. Mol. Cell. Biol. **17:**1129–1143.
17. **Master, Z., N. Jones, J. Tran, J. Jones, R. S. Kerbel, and D. J. Dumont.** 2001. Dok-R plays a pivotal role in angiopoietin-1-dependent cell migration through recruitment and activation of Pak. EMBO J. **20:**5919–5928.
18. **McNutt, N. S., V. Fletcher, and M. A. Conant.** 1983. Early lesions of Kaposi's sarcoma in homosexual men. An ultrastructural comparison with other vascular proliferations in skin. Am. J. Pathol. **111:**62–77.
19. **Mitola, S., R. Soldi, I. Zanon, L. Barra, M. I. Gutierrez, B. Berkhout, M. Giacca, and F. Bussolino.** 2000. Identification of specific molecular structures of human immunodeficiency virus type 1 Tat relevant for its biological effects on vascular endothelial cells. J. Virol. **74:**344–353.
20. **Moldovan, L., N. I. Moldovan, R. H. Sohn, S. A. Parikh, and P. J. Goldschmidt-Clermont.** 2000. Redox changes of cultured endothelial cells and actin dynamics. Circ. Res. **86:**549–557.
21. **Oshima, T., S. C. Flores, G. Vaitaitis, L. L. Coe, T. Joh, J. H. Park, Y. Zhu, B. Alexander, and J. S. Alexander.** 2000. HIV-1 Tat increases endothelial solute permeability through tyrosine kinase and mitogen-activated protein kinase-dependent pathways. AIDS **14:**475–482.
22. **Pedram, A., M. Razandi, and E. R. Levin.** 1998. Extracellular signal-regulated protein kinase/Jun kinase cross-talk underlies vascular endothelial cell growth factor-induced endothelial cell proliferation. J. Biol. Chem. **273:**26722–26728.
23. **Scheidegger, P., W. Weiglhofer, S. Suarez, S. Console, J. Waltenberger, M. S. Pepper, R. Jaussi, and K. Ballmer-Hofer.** 2001. Signalling properties of an HIV-encoded angiogenic peptide mimicking vascular endothelial growth factor activity. Biochem. J. **353:**569–578.
24. **Schwarze, S. R., and S. F. Dowdy.** 2000. In vivo protein transduction: intracellular delivery of biologically active proteins, compounds and DNA. Trends Pharmacol. Sci. **21:**45–48.
25. **Stauber, R. H., and G. N. Pavlakis.** 1998. Intracellular trafficking and interactions of the HIV-1 Tat protein. Virology **252:**126–136.
26. **Tabib, A., C. Leroux, J. F. Mornex, and R. Loire.** 2000. Accelerated coronary atherosclerosis and arteriosclerosis in young human-immunodeficiency-virus-positive patients. Coronary Artery Dis. **11:**41–46.
27. **Vogel, J., S. H. Hinrichs, R. K. Reynolds, P. A. Luciw, and G. Jay.** 1988. The HIV *tat* gene induces dermal lesions resembling Kaposi's sarcoma in transgenic mice. Nature **335:**606–611.
28. **Westendorp, M. O., R. Frank, C. Ochsenbauer, K. Stricker, J. Dhein, H. Walczak, K. M. Debatin, and P. H. Krammer.** 1995. Sensitization of T cells to CD95-mediated apoptosis by HIV-1 Tat and gp120. Nature **375:**497–500.
29. **Xu, Y. C., R. F. Wu, Y. Gu, Y. S. Yang, M. C. Yang, F. E. Nwariaku, and L. S. Terada.** 2002. Involvement of TRAF4 in oxidative activation of c-jun amino terminal kinase. J. Biol. Chem. **277:**28051–28057.
30. **Zhao, Z. S., E. Manser, X. Q. Chen, C. Chong, T. Leung, and L. Lim.** 1998. A conserved negative regulatory region in alphaPAK: inhibition of PAK kinases reveals their morphological roles downstream of Cdc42 and Rac1. Mol. Cell. Biol. **18:**2153–2163.
31. **Zietz, C., B. Hotz, M. Sturzl, E. Rauch, R. Penning, and U. Lohrs.** 1996. Aortic endothelium in HIV-1 infection: chronic injury, activation, and increased leukocyte adherence. Am. J. Pathol. **149:**1887–1898.